Attenuated *Pik3r1* Expression Prevents Insulin Resistance and Adipose Tissue Macrophage Accumulation in Diet-Induced Obese Mice

Carrie E. McCurdy,[1,2,3] Simon Schenk,[4] Michael J. Holliday,[1,2,3] Andrew Philp,[5] Julie A. Houck,[1,2,3] David Patsouris,[6] Paul S. MacLean,[2] Susan M. Majka,[2,3] Dwight J. Klemm,[2,3] and Jacob E. Friedman[1,7]

Obese white adipose tissue (AT) is characterized by large-scale infiltration of proinflammatory macrophages, in parallel with systemic insulin resistance; however, the cellular stimulus that initiates this signaling cascade and chemokine release is still unknown. The objective of this study was to determine the role of the phosphoinositide 3-kinase (PI3K) regulatory subunits on AT macrophage (ATM) infiltration in obesity. Here, we find that the *Pik3r1* regulatory subunits (i.e., p85α/p55α/p50α) are highly induced in AT from high-fat diet–fed obese mice, concurrent with insulin resistance. Global heterozygous deletion of the *Pik3r1* regulatory subunits (αHZ), but not knockout of *Pik3r2* (p85β), preserves whole-body, AT, and skeletal muscle insulin sensitivity, despite severe obesity. Moreover, ATM accumulation, proinflammatory gene expression, and ex vivo chemokine secretion in obese αHZ mice are markedly reduced despite endoplasmic reticulum (ER) stress, hypoxia, adipocyte hypertrophy, and Jun NH_2-terminal kinase activation. Furthermore, bone marrow transplant studies reveal that these improvements in obese αHZ mice are independent of reduced *Pik3r1* expression in the hematopoietic compartment. Taken together, these studies demonstrate that *Pik3r1* expression plays a critical role in mediating AT insulin sensitivity and, more so, suggest that reduced PI3K activity is a key step in the initiation and propagation of the inflammatory response in obese AT. ***Diabetes*** **61:2495–2505, 2012**

Although the pathogenesis of insulin resistance in obesity is multifactorial, it is clear that chronic, low-grade inflammation is a major contributor, with the proinflammatory macrophage identified as the primary stimulus (1). Mechanistically, the current model for insulin resistance in obesity suggests that adipose tissue macrophage (ATM) infiltration and proinflammatory cytokine release activates inflammatory pathways such as inhibitor of kappa B kinase β (IKKβ) and Jun NH_2-terminal kinase (JNK), which impinge upon the insulin signaling cascade by inhibiting tyrosine phosphorylation of insulin receptor substrate 1 (IRS1), leading to impaired insulin activation of phosphoinositide 3-kinase (PI3K) and Akt (1).

The chemoattractant stimulus and the molecular details underlying cross-talk between infiltrating macrophage and the adipocyte is an area of intense investigation. Environmental cues including adipose tissue (AT) hypoxia, cell death, physical stress on adipocyte extracellular matrix, and increased lipolysis have all been identified as mechanisms that initiate ATM recruitment, primarily through their ability to either stimulate chemokine secretion (2) or increase free fatty acid (FFA) release (3). In turn, these factors activate proinflammatory signaling cascades within the monocyte to initiate migration (3–5). A wealth of data exists linking ATM accumulation with subsequent insulin resistance in obesity (6–8). Similarly, a recent study by Lee et al. (9) found that as few as 3 days of a high fat diet (HFD) feeding in mice led to significant reduction in insulin sensitivity, which was accompanied by an increase in ATM accumulation. Interestingly, however, the decrease in insulin sensitivity after 3 days of HFD occurred independently of ATM accumulation (9).

The class 1A PI3K regulates many cellular processes, including insulin-mediated glucose transport, cell growth, apoptosis, and immune cell motility. PI3K is a heterodimeric enzyme composed of a regulatory subunit (p85α, p55α, p50α, or p85β) and a catalytic subunit (p110α or p110β) (10). Studies in cell culture and transgenic mouse models demonstrate that complete deletion of the regulatory isoforms (p85α only, p85β only, and p55α/p50α double knockout) or heterozygous *Pik3r1* deletion enhances PI3K activity and subsequent insulin sensitivity (11–14). Furthermore, inhibiting *Pik3r1* expression improves insulin signaling and glucose homeostasis in HFD-fed, obese mice (15), and mice with genetically induced insulin resistance through heterozygous loss of the IR and IRS1 (16). Several studies have identified PI3K-independent roles for the p85α subunit that may explain the inverse relationship between p85α abundance and insulin sensitivity, including activation of phosphatase and tensin homolog (PTEN) (17), nuclear translocation of X-box binding protein 1 (18,19), and activation of JNK (20).

Here, we investigated the hypothesis that maintaining insulin action can prevent ATM recruitment, even with marked obesity. To do this, we studied ATM infiltration and cytokine profiles and systemic and tissue-specific insulin sensitivity in two well-characterized PI3K regulatory subunit mouse models, the *Pik3r1* heterozygous (αHZ) mouse and

From the [1]Department of Pediatrics, University of Colorado School of Medicine, Aurora, Colorado; the [2]Department of Medicine, University of Colorado School of Medicine, Aurora, Colorado; the [3]Charles C. Gates Center for Regenerative Medicine and Stem Cell Biology, University of Colorado School of Medicine, Aurora, Colorado; the [4]Department of Orthopaedic Surgery, University of California, San Diego, La Jolla, California; the [5]Department of Neurobiology, Physiology, and Behavior, University of California Davis, Davis, California; the [6]Faculté de Médecine Lyon-Sud, INSERM U1060, Université Lyon 1, Oullins, France; and the [7]Department of Biochemistry and Molecular Genetics, University of Colorado School of Medicine, Aurora, Colorado.

Corresponding author: Carrie E. McCurdy, carrie.mccurdy@ucdenver.edu.

Received 25 October 2011 and accepted 29 January 2012.

DOI: 10.2337/db11-1433

This article contains Supplementary Data online at http://diabetes.diabetesjournals.org/lookup/suppl/doi:10.2337/db11-1433/-/DC1.

the *Pik3r2* knockout (βKO) mouse. In addition, bone marrow transplants (BMT) were performed to determine the contribution of *Pik3r1* knockdown in AT versus hematopoietic compartments to metabolism and inflammation. Our results demonstrate that obese αHZ mice, but not βKO, have significantly reduced ATM accumulation, chemokine secretion, and inflammatory gene expression. Furthermore, reducing *Pik3r1* in AT, but not in bone marrow (BM), was required to retain insulin sensitivity on HFD. These data support the contention that PI3K is a key element in the integration of signals necessary for controlling AT insulin sensitivity and the induction of the inflammatory response in AT.

RESEARCH DESIGN AND METHODS

Animal experiments and tissue collection. All studies were approved by the Institutional Animal Care and Use Committee at the University of Colorado School of Medicine. Six-week-old, male *Pik3r1*$^{+/-}$ (αHZ) and *Pik3r2*$^{-/-}$ (βKO) and their wild-type (WT) littermates were placed on an HFD (45% of calories from fat) or control diet (CON; 10% of calories from fat) from Research Diets (New Brunswick, NJ) for 16 weeks. Basal and insulin-stimulated tissue was collected as previously described (21). Blood samples were collected after a 4-h fast through the retro-orbital sinus, and plasma cytokines/adipokines were measured by multiplex assay (Bio-Rad Laboratories, Hercules, CA).

BMTs. Male C57BL/6J (CD45.1) WT recipient mice (Jackson Laboratory, Bar Harbor, ME) and male C57BL/6SVJ *Pik3r1*$^{+/-}$ (CD45.2; αHZ) recipient mice received 1,000 rads of whole-body irradiation. BM was extracted from the tibia and femur of WT *Plk3r1*$^{+/+}$ (CD45.2), WT (CD45.1), and αHZ (CD45.2) donor mice, and 2.5×10^6 cells were injected into the retro orbital sinus cavity of irradiated mice. At 6 weeks, engraftment of donor BM was tested by flow cytometry for CD45.1 or CD45.2 antigens (anti–CD45.1-PE, anti–CD45.2-APC, and ter119-FITC; BD Pharmingen) in peripheral blood (see Supplementary Fig. 3).

Hyperinsulinemic-euglycemic clamp. The hyperinsulinemic-euglycemic (H-E) clamps were conducted using two jugular vein cannulas as previously described (22), except that clamps were conducted on overnight-fasted mice that were anesthetized with a drug cocktail (acepromazine, 10 mg/mL; midazolam, 5 mg/mL; and fetanyl, 0.05 mg/mL) as previously outlined (23). This anesthesia protocol does not alter glucose metabolism during an H-E clamp (23).

Immunoblotting. Epididymal adipose tissue (eAT) was homogenized (3 g:1 mL) in ice-cold lysis buffer as previously described (22). Samples (50 μg) were run on a 7% acrylamide Bis-Tris gel and transferred to polyvinylidene fluoride membranes (Bio-Rad Laboratories). Membranes were then exposed to the appropriate primary and secondary antibodies. Glyceraldehyde-3-phosphate dehydrogenase (GAPDH) or actin was probed as a loading control.

Phosphotyrosine-associated PI3K activity. PI3K was immunoprecipitated from 500 μg AT or skeletal muscle (SkM) homogenates by incubating overnight with a mouse anti-pY100 antibody (Cell Signaling, Danvers, MA). The kinase reaction was initiated with the addition of 2 μg phosphatidylinositol (PI) and 20 μCi [γ-^{32}P]-ATP, incubated for 30 min, and then terminated by addition of 20 μL of 8 N HCL as previously described (22). The lipid products were run on a thin-layer chromatography plate, and phosphoinositol-3-phosphate [PI(3)P] was visualized on film.

Immunohistochemistry (IHC). eAT for immunohistochemistry was fixed in 10% neutral, phosphate-buffered formalin for 24–48 h and paraffin embedded, and 4-μm sections were stained with DAPI and a rat anti-mouse F4/80 monoclonal antibody (1:250; Abcam, Cambridge, MA).

RNA isolation and quantitative real-time PCR. RNA was isolated from eAT and SkM using the RNeasy Plus Mini Kit (QIAGEN, Inc., Valencia, CA). RNA was quantitated and reverse transcribed (ImPromII reverse transcriptase; Promega), and quantitative real-time PCR was run on a Roche LightCycler 480 instrument. mRNA was normalized to glyceraldehyde-3-phosphate dehydrogenase (GAPDH) or 18S. Primer sequences are presented in Supplementary Table 3.

Lipid analysis. SkM tibialis anterior (30 mg) and liver (70 mg) were lyophilized, weighed, and homogenized in MeOH along with an internal standard of tripentadecanoic acid (Omni International, Marietta, GA). SkM lipid extraction, isolation, and analysis were performed as previously described (24).

Flow cytometry. eAT was digested in Dulbecco's modified Eagle's medium (DMEM) + 0.4% collagenase I, and cells were filtered and centrifuged to collect stromal vascular cells (SVCs). Cells were incubated for 10 min with Fc block, followed by a 30-min incubation with anti–F4/80-PE and anti–CD11c-APC (eBioscience, San Diego, CA). Cells were then fixed with 1% paraformaldehyde in PBS. Analysis was performed using the FACS Calibur system with Cell Quest software.

Cell secretion assay. eAT was extracted under sterile conditions, and 1 g of tissue was minced, placed in a six-well tissue culture plate with serum-free DMEM (2 mL), and incubated for 48 h (37°C). Media was collected and stored at −80°C until use. Media was analyzed using RayBiotech, Inc. (Norcross, GA) Mouse Cytokine Array 3 according to the manufacturer's directions. Arrays were visualized on Ox-Mat film and quantitated by densitometry.

Adipocyte isolation and cell sizing. eAT was digested with 1 mg/mL collagenase type I (Sigma-Aldrich) in a Krebs-Ringer digestion buffer and isolated as previously described (25). Adipocytes were removed and immediately stained with 0.2% methylene blue for cell integrity. The imaging methods were adapted from Higgins et al. (26) using an Olympus Max U-CMAD3 microscope with digital camera and analyzed using AdCount software (Mayo Clinic, Rochester, MN).

Insulin-stimulated 2-deoxyglucose glucose uptake in adipocytes. Isolated adipocytes were washed in Krebs-Ringer phosphate buffer, spun, and distributed as 100-μL packed cells for basal or insulin-stimulated conditions. Insulin-stimulated 2-deoxyglucose (2DG) uptake was measured, as previously described (22), in the presence and absence of 1.2 nM insulin.

Insulin-stimulated 2DG uptake in SkM. Isolated-SkM, insulin-stimulated 2-DG uptake was measured in WT and αHZ extensor digitorum longus (EDL) as previously described (27). For tumor necrosis factor-α (TNF-α) experiments, the same protocol was used except that isolated EDL muscles were initially incubated in Krebs-Henseleit buffer for 1 h with or without 10 μg/mL TNF-α in the presence and absence of 0.3 nM insulin.

3T3-L1 culture experiments. 3T3-L1 preadipocytes were plated in DMEM with 1% FCS and 1 mM L-glutamate. Cells were differentiated into adipocytes by the addition of DMEM containing 10% FCS, 1 mM L-glutamate, 300 μM isobutylmethylxanthine, 1 μM dexamethasone, and 1 μg/mL insulin for 3 days. After differentiation, cells were maintained as previously described (28). For time course experiments, cells were serum starved overnight and then exposed to interleukin-6 (IL-6; 20 ng/mL) (Sigma-Aldrich) for indicated times.

Statistical analysis. Data were analyzed by two-way ANOVA for main effects of diet and genotype with Tukey post hoc analysis. Significant differences within genotype are indicated with *, and significant differences within diet group are indicated with #. Data from BMT studies were analyzed only within the HFD groups by two-way ANOVA for main effects of BM genotype and body genotype with Tukey post hoc analysis. The control group (WT/WT-CON) was used as reference to show that HFD induced a change independent of transplant. For BMT studies, * indicates significant differences within BM genotype and # indicates significant differences within body genotype. Pearson χ^2 test of independence was used to compare cell size frequency distribution profiles. 3T3-L1 adipocyte studies were analyzed by one-way ANOVA with Bonferroni post hoc test, and * indicates significant differences compared with $t = 0$.

RESULTS

Limiting *Pik3r1* expression, but not *Pik3r2*, ameliorates obesity-induced insulin resistance. After 16 weeks on HFD, αHZ and βKO, and their respective WT littermates (i.e., *Pik3r1*$^{+/+}$ and *Pik3r2*$^{+/+}$), gained significant weight compared with mice on CON, with the majority of weight gain due to an increase in body fat (Fig. 1*A* and *B*). Despite comparable obesity, whole-body insulin sensitivity was significantly greater in αHZ-HFD compared with WT-HFD mice as measured by the steady-state glucose infusion rate (GINF) during the H-E clamp (Fig. 1*C* and Supplementary Fig. 1*A*). The enhanced GINF in αHZ-HFD was primarily due to an increase in insulin-stimulated glucose disposal rate (IS-GDR), as suppression of hepatic glucose production by insulin was not different between αHZ-HFD and WT-HFD (Fig. 1*D* and *E* and Supplementary Fig. 1*B*). AT insulin sensitivity, measured by the ability of insulin to suppress FFA and glycerol levels during the clamp, was significantly impaired in WT-HFD mice, but was similar to CON in αHZ-HFD mice (Fig. 1*F* and *G* and Supplementary Fig. 1*C* and *D*). Surprisingly, the metabolic improvements did not manifest in βKO-HFD mice, which were indistinguishable from WT-HFD mice (Fig. 1*C*–*G* and Supplementary Fig. 1*A*–*D*). Supporting the clamp data,

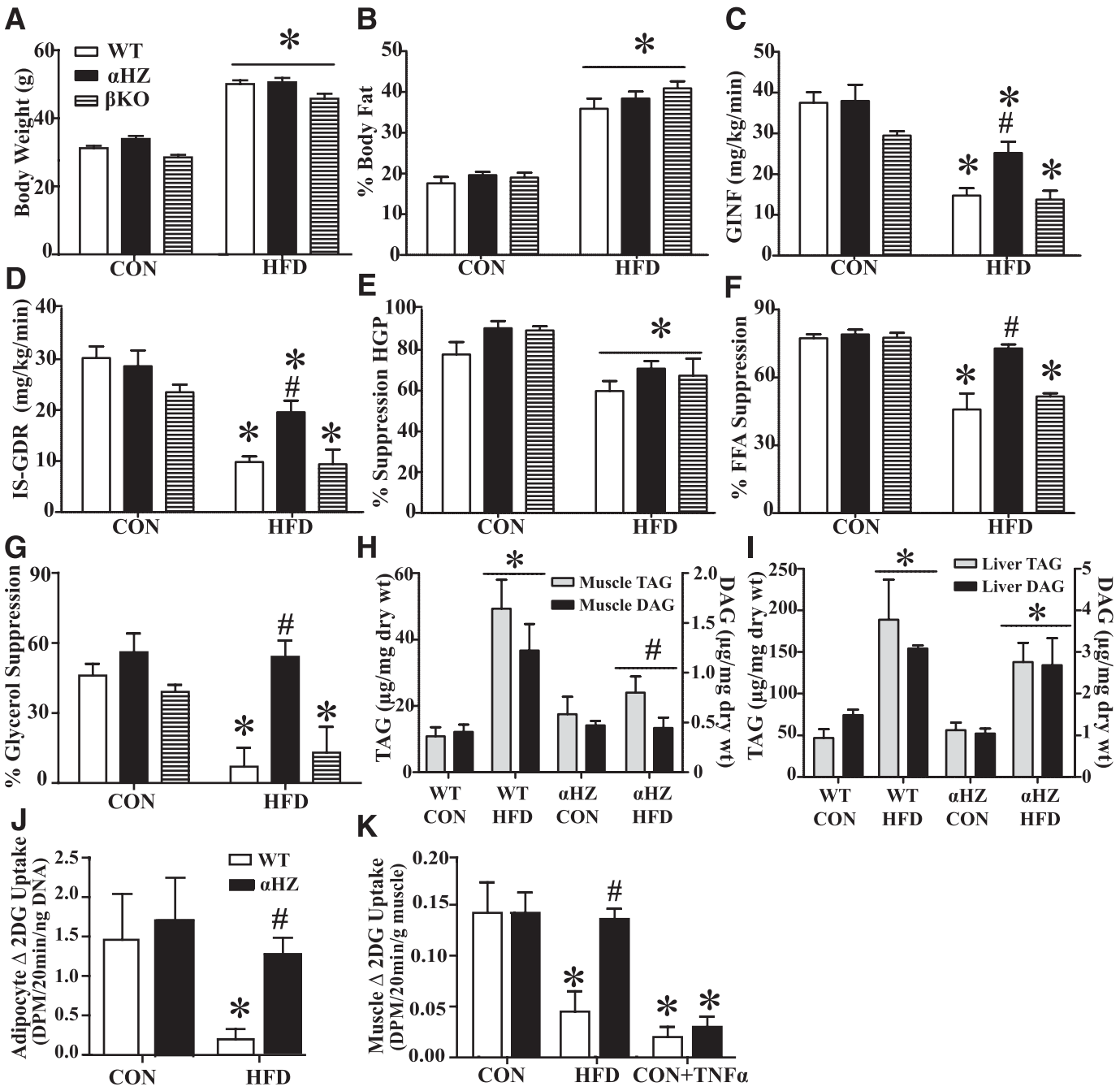

FIG. 1. Partial deletion of *Pik3r1*, but not *Pik3r2*, improves insulin sensitivity in obese mice. *A*: Body weight data at 16 weeks for WT, αHZ, and βKO mice fed a control (CON) or 45% HFD. *n* = 20 per group. *B*: Percent body fat determined by dual-energy X-ray absorptiometry. *C*: GINF. *D*: IS-GDR. *E*: Percent suppression of hepatic glucose production (HGP). Free fatty acids (*F*) and glycerol (*G*) were measured during the H-E clamp (insulin infusion, 12 mU insulin/kg/min). *n* = 6–10 per group. SkM (*H*) and liver triglyceride (*I*) (TAG; left *y*-axis) and diacylglyceride (DAG; right *y*-axis) concentration were measured by mass spectrophotometry in WT and αHZ mice after diet exposure. *n* = 5 per group. Insulin-stimulated 2DG uptake was measured in isolated adipocytes (*J*) and isolated EDL muscles (*K*) preincubated with or without 10 μg/mL TNF-α from WT and αHZ mice after diet exposure (*n* = 3–5 per group). All data are mean + SEM. Data were analyzed by two-way ANOVA for main effects of diet and genotype with a Tukey post hoc test. *$P < 0.05$ within same genotype and #$P < 0.05$ within same diet group compared with WT.

lipid analysis of SkM showed a significant twofold increase in triglyceride and diacylglyceride concentrations in WT-HFD, but not αHZ-HFD, compared with CON-fed mice, consistent with improved IS-GDR in αHZ-HFD (Fig. 1*H*). Hepatic triglycerides and diacylglycerides were elevated twofold in both WT and αHZ on HFD (Fig. 1*I*). In isolated adipocytes (Fig. 1*J*) and SkM (Fig. 1*K*), again, WT-HFD, but not αHZ-HFD, had reduced insulin-stimulated 2DG uptake. Because AT inflammatory cytokine secretion is thought to drive systemic insulin resistance, we measured insulin sensitivity in isolated EDL muscles after exposure to TNF-α. Insulin-stimulated 2DG uptake in the EDL was equally reduced in WT and αHZ after TNF-α treatment (Fig. 1*K*), which suggests that improved SkM insulin sensitivity in αHZ-HFD may occur secondary to reduced systemic levels of inflammatory cytokines.

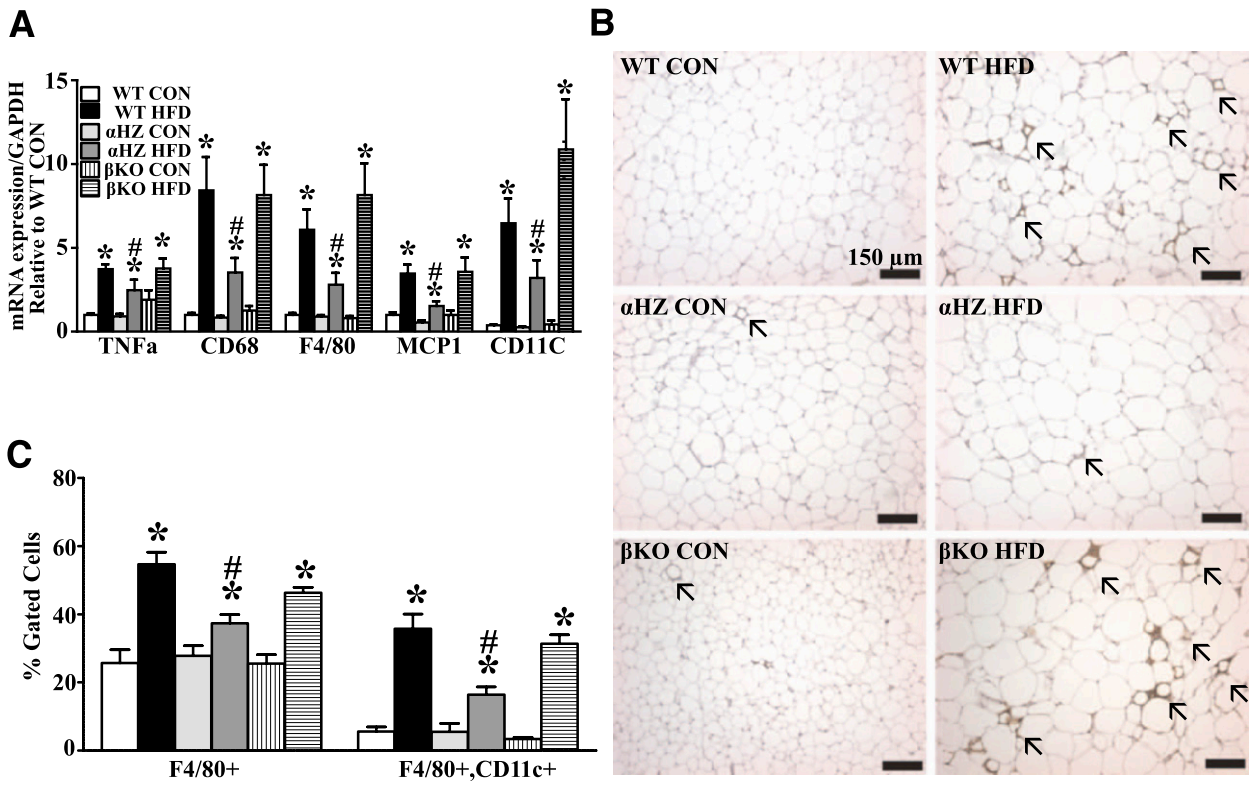

FIG. 2. Reduced AT inflammation and ATM accumulation in αHZ-HFD mice. *A*: Inflammatory and macrophage gene expression were measured by quantitative PCR in eAT. Data are mean + SEM. *n* = 5–6 per group. *B*: Representative sections of eAT were immunostained with F4/80 and DAPI nuclear stain. Arrows point to F4/80+ crown-like structures. *C*: eAT was digested to isolate cells from the SVF. *n* = 6–8 per group. SVF cells were incubated with antibodies for F4/80 and CD11c and quantitated by flow cytometry. Data are presented as mean percent of antigen-positive cells ± SEM within the live cell gate. A two-way ANOVA for main effects of diet and genotype was used for statistical analysis with a Tukey post hoc test. *$P < 0.05$ within same genotype and #$P < 0.05$ within same diet group compared with WT. (A high-quality digital representation of this figure is available in the online issue.)

Obese *Pik3r1*$^{+/-}$ mice have reduced AT inflammation and macrophage accumulation. Inflammatory and macrophage markers were significantly elevated in AT and SkM from all groups compared with their respective CON groups, but were greatly reduced in αHZ-HFD vs. WT-HFD (Fig. 2*A* and Supplementary Fig. 2). Paralleling these changes, more F4/80+ cells were present in characteristic crown-like structures in WT-HFD and βKO-HFD, but not αHZ-HFD, compared with WT-CON (Fig. 2*B*). By flow cytometry, we found significant, two- and sevenfold increases in F4/80+ and F4/80+/CD11c+ cells, respectively, in the SVC fraction of WT-HFD and βKO-HFD versus WT-CON (Fig. 2*C*). In contrast, there were significantly less F4/80 + and F4/80+/CD11c+ cells in AT from αHZ-HFD compared to WT-HFD (Fig. 2*C*). Representative gated flow cytometry scatter plots with average percent of cells per quadrant for each group are presented in Supplementary Fig. 3.

Plasma insulin and some proinflammatory cytokine levels are reduced in obese *Pik3r1*$^{+/-}$ mice. Plasma insulin, resistin, and plasminogen activator inhibitor-1 were significantly elevated in WT-HFD versus WT-CON mice, but not in αHZ-HFD mice. Additionally, plasma adiponectin levels were significantly decreased in WT-HFD, but not αHZ-HFD, mice as compared with CON (Table 1). Chemokine (C-C motif) ligand (CCL) 2 (CCL2)/monocyte chemotactic protein-1 (MCP-1) was not increased in the plasma of HFD mice; however, both IL-6 and leptin were significantly increased in HFD, regardless of genotype (Table 1).

TABLE 1
Fasting plasma metabolic factors

	WT-CON	WT-HFD	αHZ-CON	αHZ-HFD
Insulin (ng/mL)	0.35 ± 0.1	1.0 ± 0.1*,†	0.49 ± 0.17	0.73 ± 0.12
Glucose (mg/dL)	76.1 ± 6.1	81.9 ± 7.3	69.3 ± 2.4	72.8 ± 7.2
Leptin (pg/mL)	2,891.0 ± 736.5	7,878.2 ± 321.2*	2,053.1 ± 446.6	7,737.0 ± 758*
MCP-1 (pg/mL)	64.9.0 ± 1.6	63.9 ± 2.0	61.9 ± 3.6	62.1 ± 2.5
Resistin (pg/mL)	3,436.2 ± 451.2	5,672.8 ± 901.6*	4,428.8 ± 586.6	5,370.2 ± 587.7
IL-6 (pg/mL)	16.3 ± 0.7	28.8 ± 3.8*	18.7 ± 2.2	25.7 ± 4.3*
PAI-1 (pg/mL)	403.6 ± 81.8	1,181.0 ± 57.3*,†	553.6 ± 89.6	413.6 ± 40.8
Adiponectin (mg/mL)	34.27 ± 1.5	25.74 ± 1.9*,†	35.11 ± 2.6	32.63 ± 1.3

Plasma factors were measured using Multiplex ELISA or a standard ELISA for insulin. Data presented as mean ± SEM. MCP-1, monocyte chemotactic protein-1. PAI-1, plasminogen activator inhibitor-1. *$P < 0.05$ within same genotype. †$P < 0.05$ within same diet group.

TABLE 2
Cytokine and chemokine levels in conditioned media from AT explants

	WT-CON	WT-HFD	αHZ-HFD
AXL	**36 ± 1**	**61 ± 8***	**33 ± 5†**
CXCL13	**41 ± 4**	**51.0 ± 5**	**26 ± 5†**
CD40	35 ± 1	50 ± 8	24 ± 3
CRG-2	**35 ± 2**	**48 ± 7**	**23 ± 4†**
CTACK	49 ± 5.4	61 ± 3.1	39 ± 6
CXCL16	**80 ± 2**	**183 ± 14***	**129 ± 12†**
FAS ligand	25 ± 1	32 ± 6	23 ± 5
G-CSF	134 ± 35	261 ± 37	215 ± 20
GM-CSF	51 ± 11	50 ± 10	27 ± 20
IFN-γ	37 ± 9	34 ± 14	29 ± 5
IGF-BP6	**71 ± 3**	**139 ± 14***	**59 ± 7†**
IL-1α	**69 ± 7**	**70 ± 6**	**43 ± 5†,***
IL-1β	**41 ± 1**	**52 ± 10**	**26 ± 2†,***
IL-2	39 ± 3	51 ± 9	25 ± 2
IL-3	**40 ± 1**	**39 ± 3**	**23 ± 2†,***
L-selectin	**72 ± 4**	**65 ± 11***	**58 ± 1†**
MCP-1	381 ± 62	399 ± 25	285 ± 55
MCP-5	39 ± 3	32 ± 5	19 ± 10
M-CSF	**107 ± 38**	**188 ± 25***	**65 ± 19†**
MIG/CXCL9	37 ± 21	47 ± 11	301 ± 5
MIP-1α/CCL3	41 ± 17	27 ± 7	28.± 13
CXCL4	**61 ± 14**	**118 ± 10***	**65 ± 8†**
P-selectin	86 ± 18	94 ± 12	94 ± 7
RANTES/CCL5	77 ± 22	87 ± 54	35 ± 7
CXCL12α	**26 ± 4**	**58 ± 9***	**26 ± 5†**
TARC/CCL17	28 ± 1	39 ± 4	26 ± 5
CCL1	**48 ± 12**	**88 ± 3***	**48 ± 5†**
TECK/CCL25	30 ± 1	47 ± 13	25 ± 4
TIMP-1	**75 ± 7**	**92 ± 3**	**51 ± 4†,***
TNF-α	30 ± 9	17 ± 0.3	29 ± 4.6
sTNF RI	241 ± 47	324 ± 24	332 ± 19
sTNF RII	**76 ± 3**	**146 ± 21***	**189 ± 14***
VCAM-1	**180 ± 3**	**304 ± 16***	**323 ± 24***

Media from AT explants was analyzed by immunoblot assay. Data (presented as mean ± SEM) are expressed relative to an internal positive control. Values in bold indicate a statistical difference. *$P < 0.05$ vs. WT-CON. †$P < 0.05$ vs. WT-HFD. CD40, cluster of differentiation (CD) 40; CRG-2, cytokine responsive gene-2; CTACK, cutaneous T-cell attracting chemokine; Fas, also known as CD95; G- and GM-CSF, granulocyte- and granulocyte-macrophage colony stimulating factor (CSF); IFN, interferon; IGFBP6, insulin like growth factor binding protein 6; MCP-1 and -5, monocyte chemotactic protein-1 and -5; M-CSF, macrophage-CSF; MIG/CXCL9, monokine-induced by interferon/chemokine (C-X-C motif) ligand (CXCL) 9; MIP-1α/CCL3, macrophage inflammatory protein-1α/chemokine (C-C motif) ligand (CCL) 3; RANTES, regulated upon activation, normal T-cell expressed and secreted; TARC, thymus and activated regulated chemokine; TECK, thymus expressed chemokine; TIMP-1, tissue inhibitor of metalloproteinases 1; sTNF RI and RII, soluble tumor necrosis factor receptor I and receptor II; VCAM-1, vascular cell adhesion molecule-1.

Secretion of chemotactic factors from AT is significantly reduced in αHZ-HFD mice. We profiled media collected from αHZ-HFD, WT-HFD, and WT-CON AT explants. Of the 62 cytokines measured, 10 inflammatory chemokines were differentially secreted in AT from WT-HFD versus αHZ-HFD mice (Table 2). Six of these secreted factors, chemokine (C-X-C motif) ligand (CXCL) 13 (CXCL13), CXCL12, CXCL4, CXCL16, CCL1, and L-selectin are chemoattractants for immune cells (2,29,30) and were elevated in WT-HFD but not αHZ-HFD. Macrophage colony stimulating factor (M-CSF), a cytokine that stimulates macrophage differentiation (31), and CXCL10, a proinflammatory cytokine released by macrophages (32), were also increased in conditioned media from WT-HFD only. IL-1α, IL-3, and tissue inhibitor of metalloproteinases 1 (TIMP-1) were differentially secreted in αHZ-HFD as compared with WT mice in a pattern that would positively influence extracellular matrix (ECM) remodeling and collagen synthesis (33,34). The full list of secreted factors can be found in Supplementary Table 1. Paralleling the changes in cytokine secretion, phosphorylation of IKKα/β(S180/181) in AT was increased twofold in WT-HFD versus WT-CON, but was not increased in αHZ-HFD (Supplementary Fig. 7*A*).

Greater adipocyte size in βKO and αHZ versus WT mice with HFD feeding. Adipocytes from HFD versus CON were larger in size but fewer in number (Supplementary Fig. 4*A–D*). In CON groups, a greater percentage of αHZ adipocytes were larger than WT, whereas βKO had a greater percentage of cells that were smaller (Supplementary Fig. 4*A* and *B*). In HFD groups, αHZ and βKO had a greater percentage of larger adipocytes compared with WT (Supplementary Fig. 4*A* and *B*). Notably, despite the larger cell size in both αHZ-HFD and βKO-HFD, only the αHZ-HFD mice were protected against ATM infiltration and adipocyte insulin resistance.

The protective effect of *Pik3r1* knockdown on insulin sensitivity and ATM infiltration is independent of the hematopoietic compartment. BMT studies were performed in lethally irradiated *Pik3r1*$^{+/-}$ and WT mice. We created four chimeras: WT BM into WT mice (WT→WT; donor BM genotype→recipient mouse genotype), *Pik3r1*$^{+/-}$ BM into WT mice (αHZ→WT), *Pik3r1*$^{+/-}$ BM into *Pik3r1*$^{+/-}$ mice (αHZ→αHZ), and WT BM into *Pik3r1*$^{+/-}$ mice (WT→αHZ) (Fig. 3*A*). Flow cytometry on peripheral blood monocytes shows that engraftment was complete within 6 weeks of transplant (Supplementary Fig. 5*A–D*). Mice with >80% engraftment were placed on an HFD for 12 weeks and insulin sensitivity was measured by clamp. Body weight and percent body fat were significantly increased in all BMT-HFD mice compared with WT→WT-CON mice (Fig. 3*B–C*). Insulin sensitivity (GINF) was not impaired in obese αHZ→αHZ-HFD, but was significantly reduced in WT→WT-HFD mice versus WT→WT-CON (Fig. 3*D*). Replacing WT BM with *Pik3r1*$^{+/-}$ BM did not improve insulin sensitivity in obese WT mice (αHZ→WT), and GINF was similar to WT→WT-HFD mice (Fig. 3*D*). Replacing *Pik3r1*$^{+/-}$ BM with WT BM did not impair insulin sensitivity as GINF in WT→αHZ-HFD was similar to αHZ→αHZ-HFD mice (Fig. 3*D*).

Complementing the insulin sensitivity data, gene expression of inflammatory and macrophage markers in AT was significantly increased in WT→WT-HFD and αHZ→WT-HFD mice compared with WT→WT-CON, but were attenuated in αHZ→αHZ-HFD and WT→αHZ-HFD mice (Fig. 4*A*). In addition, only AT from WT→WT-HFD and αHZ→WT-HFD mice had a significant increase in F4/80+ cells forming crown-like structures by immunohistochemistry and more F4/80+ (approximately twofold) and F4/80+/CD11c+ (approximately eightfold) cells counted in the SVCs compared with WT→WT-CON mice (Fig. 4*B* and *C*). Macrophage infiltration was markedly reduced and essentially absent in WT→αHZ-HFD and αHZ→αHZ-HFD mice (Fig. 4*B* and *C*).

Proximal insulin signaling, but not PI3K-Akt signaling, is impaired in AT from obese αHZ mice. Insulin-stimulated tyrosine phosphorylation of IRS1 (pIRS1[Y612]) was significantly and equally impaired (approximately threefold) in

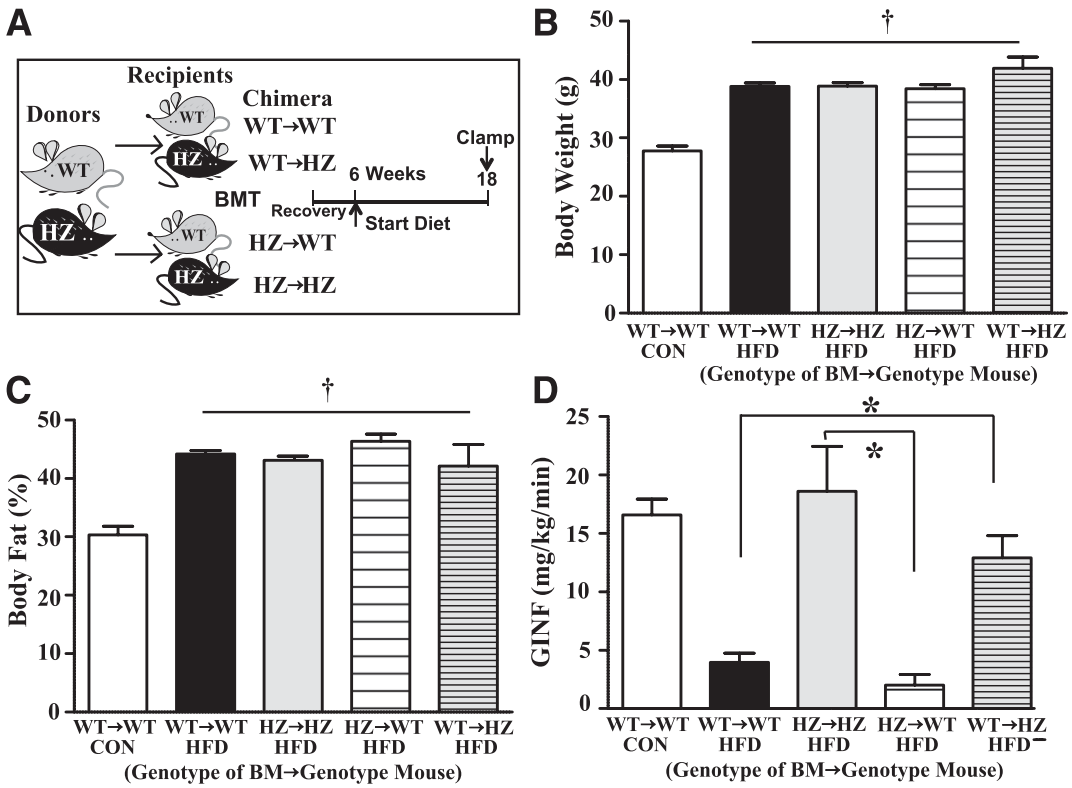

FIG. 3. Increased insulin sensitivity in obese αHZ mice is independent of *Pik3r1*$^{+/-}$ in hematopoietic cells. *A*: Schematic of BMT study design and mouse groups. Body weight (*B*) and percent body fat (*C*) were measured by dual-energy X-ray absorptiometry analysis after 12 weeks on CON or HFD. †$P < 0.05$ compared with WT→WT-CON for *B* and *C*. *D*: GINF during the clamp (insulin infusion, 6 mU insulin/kg/min). All data are mean + SEM. $n = 6–8$ per group. Data were analyzed by a two-way ANOVA for main effects within the HFD group for BM genotype and body genotype with a Tukey post hoc test. *$P < 0.05$ within same BM genotype. The WT→WT-CON is included as a reference to show effects of HFD.

AT of all HFD versus CON mice (Fig. 5*A* and *B* and Supplementary Fig. 6*A*). The decrease in IRS1 activation was accompanied by a significant reduction (~50%) in IRS1 abundance (Fig. 5*A* and Supplementary Fig. 6*A*). This reduction was likely due to increased IRS1 serine phosphorylation as JNK1(T138/Y185) phosphorylation was equally upregulated in AT from WT-HFD and αHZ-HFD mice (Supplementary Fig. 7*B*). X-box binding protein 1 splicing and gene expression of the ER stress markers growth arrest and DNA damage-inducible gene-153 (GADD153) and glucose-regulated protein, 78kDa (GRP78) and hypoxia markers, vascular endothelial growth factor (VEGF), GLUT1, and hypoxia-inducible factor (HIF) 1α, were elevated in AT with HFD regardless of genotype (Supplementary Fig. 7*C–E*). These findings are important in that the decrease in IRS1 activation and upregulation of pJNK1(T138/Y185), ER stress, and hypoxia occurred without profound ATM accumulation in αHZ-HFD. Despite reduced insulin-stimulated IRS1 activation, insulin-stimulated Akt(S473) and Akt(T308) phosphorylation was not impaired in αHZ-HFD, but was impaired in WT-HFD versus CON mice (Fig. 5*A*, *D*, and *E*). Enhanced insulin-stimulated Akt activation did not occur in βKO-HFD mice (Supplementary Fig. 6*A*). Insulin-stimulated, pY-associated PI3K activity in AT was also reduced twofold in WT-HFD versus WT-CON mice, but was not reduced in αHZ-HFD mice (Fig. 5*F*). There was no difference in basal pY-associated PI3K activity (Fig. 5*F*).

Pik3r1 abundance is increased in AT from WT-HFD but not αHZ-HFD mice. In parallel with the insulin-stimulated PI3K activity, there was a significant increase in the abundance of the shorter isoforms of *Pik3r1* (p55α and p50α; four- and twofold, respectively) and a smaller (40%) increase in p85α in AT from WT-HFD and βKO-HFD versus WT-CON, which did not occur in αHZ-HFD mice (Fig. 5*A* and *C* and Supplementary Fig. 6*A*). Changes in p55α/p50α abundance in WT-HFD were paralleled by an increase in mRNA levels of *p55α* and *p50α*, but not *p85α* (Supplementary Fig. 7*F*). p110α abundance was not different across groups (Fig. 5*A*). Interestingly, we observed only a modest, nonsignificant decrease in p85α abundance in AT from *Pik3r1*$^{+/-}$ mice despite a significant, 50% decrease in mRNA expression, suggesting that *Pik3r1* protein stability is likely increased. We speculate that increased protein stability may be due to a greater number of the *Pik3r1* regulatory subunits binding to the catalytic subunit to form heterodimers or to other p85α binding partners. Indeed, association with the catalytic subunit has been previously shown to increase heterodimer stability (35). Thus, these data suggest that HFD appears to reduce insulin-stimulated PI3K activity and downstream signaling to Akt, at least in part through upregulation of p85α, p55α, and p50α expression and protein abundance in AT.

SkM insulin signaling is not impaired in αHZ-HFD mice. Despite severe obesity, SkM insulin signaling was not impaired in αHZ-HFD mice compared with αHZ-CON, whereas WT-HFD mice had significant impairments in insulin-stimulated tyrosine phosphorylation of pIRS1(Y612) (~50%), insulin-stimulated pY-associated PI3K activity, and Akt(S473) phosphorylation compared with WT-CON (Supplementary Fig. 8*A*, *B*, *E*, and *F*). Similar to AT, p85α

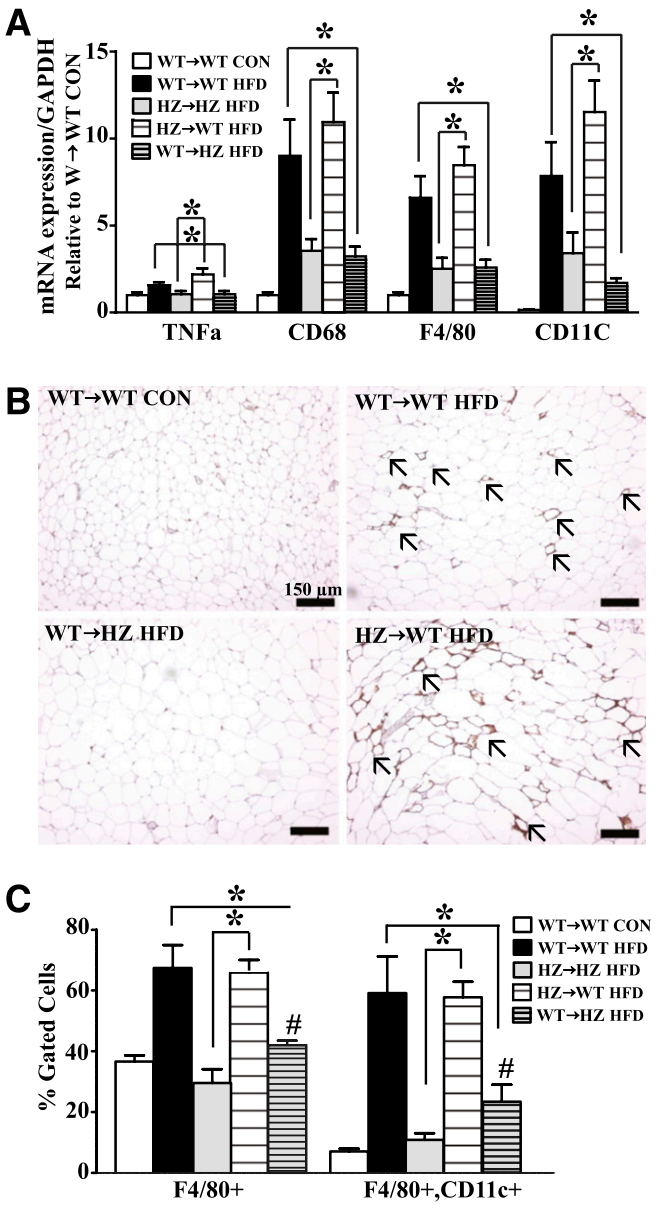

FIG. 4. Reduced AT inflammation and macrophage accumulation in αHZ-HFD are independent of hematopoietic compartment. *A*: Inflammatory and macrophage gene expression measured by quantitative PCR in eAT from BMT mice. *B*: Representative sections of eAT were immunostained with F4/80. Arrows point to F4/80+ crown-like structures. *C*: Cells from the SVF of the AT were isolated, incubated with antibodies for F4/80 and CD11c, and quantitated by flow cytometry. All data are mean + SEM. n = 6–8 per group. Data were analyzed by a two-way ANOVA for main effects within the HFD group for donor BM genotype and recipient body genotype with a Tukey post hoc test. *$P < 0.05$ within same BM genotype and #$P < 0.05$ within same body genotype. The WT→WT-CON is included as a reference to show effects of HFD. (A high-quality digital representation of this figure is available in the online issue.)

abundance was increased in WT-HFD SkM, with no change in p110 abundance (Supplementary Fig. *C–E*). Although there was no significant decrease in p85α abundance in αHZ SkM, we did find an ~50% decrease in the p110α catalytic subunit (Supplementary Fig. *C–E*). This decrease in p110 abundance was reflected in a 50% decrease in insulin-stimulated, pY-associated PI3K activity in both αHZ-CON and αHZ-HFD SkM; however, correcting for catalytic subunit abundance in all groups, insulin-stimulated, pY-associated PI3K activity/p110 was significantly higher in αHZ groups compared with their diet-matched WT group (Supplementary Fig. 6*F*). The adjusted insulin-stimulated PI3K activity matches the increase in Akt phosphorylation seen in αHZ mice compared with WT groups (Supplementary Fig. 8*B* and *F*).

STAT3 activation in AT parallels increased p55α/p50α expression. Nuclear localization of signal transducer and activator of transcription 3 (STAT3) (Fig. 6*A*) was increased in AT of WT-HFD and αHZ-HFD versus WT-CON. Because IL-6 was elevated in both WT-HFD and αHZ-HFD and is known to activate STAT3 (36), we studied the effects of IL-6 treatment on *p85α*, *p55α*, and *p50α* expression in differentiated 3T3-L1 adipocytes. IL-6 rapidly activated STAT3(Y705) phosphorylation within 15 min (Fig. 6*B*), corresponding to an acute rise in STAT3 genes *IL-6* and *SOCS3* (Fig. 6*C*). Interestingly, STAT3 activation by IL-6 appeared biphasic, with peak phosphorylation at 1 and 24 h (Fig. 6*B*). This pattern of activation suggests the possibility that acute IL-6 stimulation of STAT3 may lead to secretion of a second factor that then reactivates STAT3 signaling. Only chronic IL-6 stimulation led to a significant increase in *p55α* and *p50α* expression (Fig. 6*D*). No increase in *p85α* expression was found in response to IL-6 stimulation (Fig. 6*D*).

DISCUSSION

Despite strong evidence for a link between macrophage accumulation in AT and insulin resistance in obesity, the factors that initiate chemokine secretion for macrophage recruitment remain elusive. In this study, we introduce the idea that AT insulin resistance is an important factor that links cellular metabolism, particularly insulin action, to chemokine secretion and initiation of macrophage recruitment.

Elegant transgenic mouse studies have demonstrated that AT inflammation and macrophage chemotaxis are reduced when signaling pathways, such as JNK, toll-like receptor 4, and IKK, are manipulated in the hematopoietic compartment (6–8). The underlying conclusion from these and comparable studies (1) is that AT inflammation is driven by macrophage infiltration, and secondary to this infiltration, AT insulin resistance manifests. In contrast, however, several studies have found dissociation between ATM infiltration and the development of insulin resistance. For example, in lean mice null for transforming growth factor-β receptor and apolipoprotein E, there is massive T-cell activation, hyperlipidemia, ATM infiltration, and up-regulation of inflammatory cytokines but no evidence of adipocyte or systemic insulin resistance (37). In our study, AT from WT-HFD had significant increases in F4/80+ and F4/80+/CD11c+ cells, whereas accumulation of these cells in AT was attenuated in αHZ-HFD mice. Our BMT experiments demonstrate that the metabolic improvements in αHZ-HFD mice are independent of changes in *Pik3r1* expression in myeloid cells. In fact, even when αHZ mice were transplanted with WT BM (WT→αHZ), which would be expected to facilitate F4/80+/CD11c+ infiltration and AT inflammation in obese mice, F4/80+/CD11c+ cells were significantly reduced compared with obese WT→WT mice. Taken together, these experiments demonstrate that the impact of reduced PI3K regulatory subunits on improved insulin sensitivity and macrophage recruitment in obese *Pik3r1*$^{+/-}$ mice is driven by non-hematopoietic–derived cells.

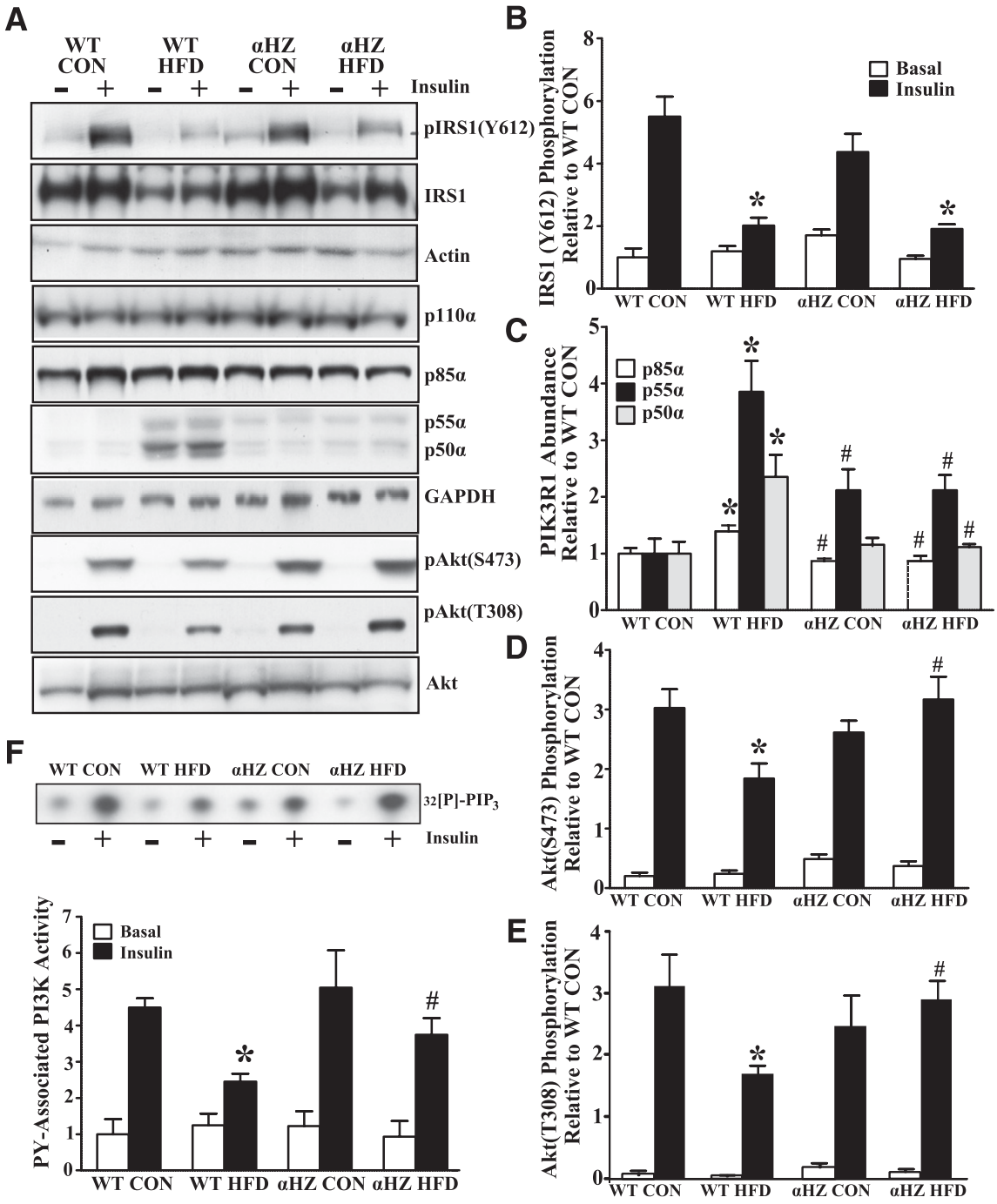

FIG. 5. Proximal insulin signaling but not PI3K/Akt signaling is impaired in AT from obese αHZ-HFD mice. Insulin signaling protein abundance and activation were measured in eAT before and after maximal insulin stimulation in WT and αHZ mice. *A*: Representative immunoblots are shown. Quantitation of signaling proteins from immunoblots for IRS1(Y612) phosphorylation (*B*), p85/55/50α abundance (*C*), Akt(S473) phosphorylation (*D*), Akt(T308) phosphorylation (*E*), and PY-associated PI3K activity (*F*) was assayed in basal and insulin-stimulated eAT. Data shown as the mean + SEM. *n* = 6–10 per group. Data were analyzed by two-way ANOVA for main effects of diet and genotype with a Tukey post hoc test. **P* < 0.05 within same genotype and #*P* < 0.05 within same diet group.

Local hypoxia, upregulation of proinflammatory JNK1 and IKKβ pathways, and induction of ER stress have all been shown to be key signaling pathways that contribute to AT insulin resistance, primarily through inhibition of insulin signaling at the level of IRS1 (1). We found that activation of JNK, ER stress, and hypoxia were induced similarly in AT from WT-HFD, βKO-HFD, and αHZ-HFD mice, in parallel with reduced insulin-stimulated activation of IRS1. Despite these changes in IRS1, insulin-stimulated PI3K activity was not reduced in AT from αHZ-HFD mice but was impaired in WT-HFD. Thus, these data demonstrate that partial deletion of *Pik3r1*, and subsequent maintenance of PI3K function, bypasses the obesity- and inflammation-mediated reductions in tyrosine activation of IRS1. Moreover, our results clearly demonstrate that PI3K-dependent signaling is critical for ATM recruitment in obesity. A separate study found that increased AT lipolysis leads to a rapid increase in ATM accumulation in lean mice

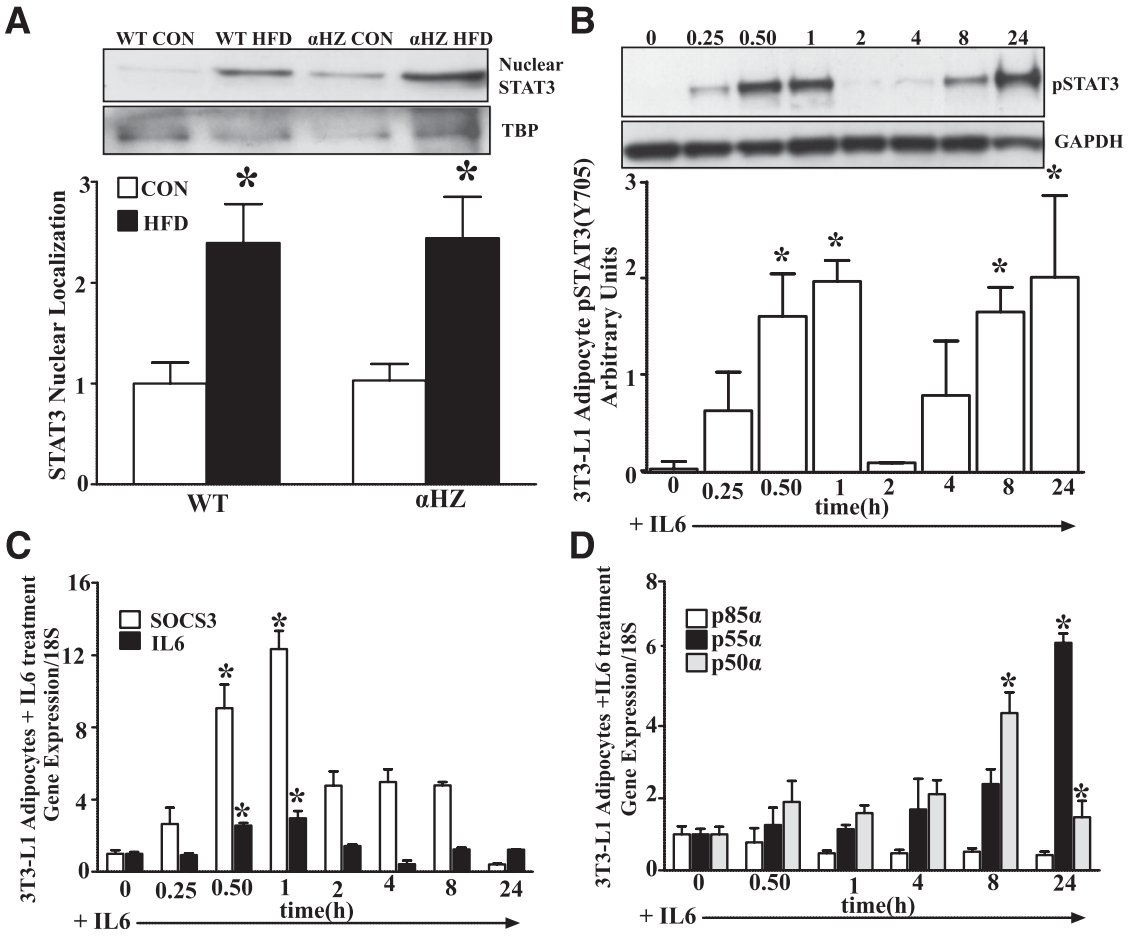

FIG. 6. STAT3 activation may underlie increased p55α/p50α expression in AT. *A*: AT nuclear STAT3 abundance was measured by immunoblot assay in lean and obese WT and αHZ mice. Differentiated 3T3-L1 adipocytes were exposed to 20 ng/mL IL-6, and STAT3(Y705) phosphorylation (*B*) was measured by immunoblot assay, and STAT3-activated genes *SOCS3* and *IL-6* (*C*) and p85α, p55α, and p50α (*D*) by quantitative PCR in cell lysates at indicated times. $n = 2$ experiments in triplicate. One-way ANOVA with Bonferroni post hoc was used for statistical analysis. *$P < 0.05$ vs. baseline.

after fasting or after initial weight loss in HFD-fed mice, suggesting that increased FFA may be an important cue for macrophage recruitment (38). Like the findings of Kosteli et al. (38), αHZ-HFD mice had no impairments in insulin suppression of FFAs or glycerol during a clamp and significantly less ATM accumulation as compared with WT-HFD mice, which failed to suppress lipolysis during the clamp. Mechanistically, we believe that the local tissue environment plays a major role in reducing ATM recruitment in *Pik3r1*$^{+/-}$ mice. To this end, AT explants from αHZ-HFD mice secreted less proinflammatory cytokines compared with WT-HFD mice. This reduction in chemokine and cytokine secretion may be linked to the reduction in IKK (S180/S181) phosphorylation in AT from αHZ-HFD compared with WT-HFD mice. Activation of IKKβ is thought to be a key regulator of inflammatory gene expression in obesity through regulation of nuclear factor-κB activity (7). Alternatively, reduced inflammation in αHZ-HFD compared with WT-HFD mice may be linked to the increased circulating adiponectin, which has potent anti-inflammatory effects (39).

Although PI3K is a key regulator of insulin signaling, surprisingly, little is known about the signaling mechanisms that modulate the expression of the regulatory subunits of PI3K in response to nutrient flux. Increased expression of *p85α* in peripheral tissues occurs in response to increased insulin (40), growth hormone (21), and dexamethasone (41). Additionally, rosiglitazone increases *p85α* expression in human adipocytes through peroxisome proliferator–activated receptor γ activation (42), and SkM *p85α* expression is strongly induced by peroxisome proliferator–activated receptor α activation (43). We speculate that the increase in p85α in WT-HFD AT and SkM may be due to increased fasting insulin in WT-HFD mice. Regarding p55α/p50α transcription, Abell et al. (44) reported that STAT3 activation increases p55α/p50α transcription during mammary gland differentiation, stimulating apoptosis through inhibition of PI3K activity. A similar pattern of PI3K regulation has recently been proposed in SkM in response to caloric restriction (22). In agreement, we found that AT p55α/p50α abundance was increased in parallel with increased STAT3 nuclear localization in WT-HFD mice and in 3T3-L1 cells in response to chronic IL-6 exposure. Limiting STAT3 transcription of *Pik3r1* in AT could be an attractive target for preventing obesity-induced insulin resistance. In support of this, mice with AT-specific knockout of STAT3 have increased body weight and adiposity with no impairment in insulin sensitivity (45).

In summary, our results suggest that impaired AT insulin sensitivity in obesity at the level of PI3K is a critical step necessary for ATM infiltration and inflammation. Moreover, they suggest a model in which reduced PI3K function and

AT insulin resistance manifests due to increased adipocyte activation of STAT3 and *p55α/p50α* transcription. These data also raise new questions as to whether the reduced inflammatory response in AT of *Pik3r1*$^{+/-}$ mice is due directly to improvements in insulin action or, alternatively, related to improved PI3K activity independent of the insulin signaling pathway. Thus, the molecular mechanism of how PI3K signaling affects macrophage function remains to be further defined; however, the present results suggest that modulating AT *Pik3r1* expression and PI3K function is a potentially attractive avenue for the development of novel therapies to treat AT insulin resistance and inflammation in obesity.

ACKNOWLEDGMENTS

This work was supported by grants from the National Institutes of Health (P30-DK-048520 and P30-DK-57516 to C.E.M., P30-AR-058878 and R24 HD050837 to S.S., DK-059767 to J.E.F., and DK-053969 to D.J.K.) and the Agence Nationale de la Recherche (ANR-09-RPDOC-018-01 to D.P.). C.E.M. is supported by the Office of Research in Women's Health (K12-HD-057022).

No potential conflicts of interest relevant to this article were reported.

C.E.M., S.S., and A.P. researched data, contributed to the discussion, and wrote and edited the manuscript. M.J.H. and J.A.H. researched data and contributed to the discussion. D.P., P.S.M., S.M.M., and D.J.K. researched data, contributed to the discussion, and edited the manuscript. J.E.F. contributed to the discussion and edited the manuscript. C.E.M. is the guarantor of this work and, as such, had full access to all the data in the study and takes responsibility for the integrity of the data and the accuracy of the data analysis.

Parts of this study were presented in abstract form at the 70th Scientific Sessions of the American Diabetes Association, Orlando, Florida, 25–29 June 2010, and at the 68th Scientific Sessions of the American Diabetes Association, San Francisco, California, 6–10 June 2008.

The authors thank Dr. C. Ronald Kahn (Joslin Diabetes Center at Harvard Medical School, Boston, MA) for providing the transgenic mice used in this study, Dr. Jerrold M. Olefsky (University of California, San Diego) for guidance, and Keith J. Fox and Heidi Miller (University of Colorado School of Medicine) for technical assistance with 3T3-L1 adipocyte cultures.

REFERENCES

1. Olefsky JM, Glass CK. Macrophages, inflammation, and insulin resistance. Annu Rev Physiol 2010;72:219–246
2. Smith H, Whittall C, Weksler B, Middleton J. Chemokines stimulate bidirectional migration of human mesenchymal stem cells across bone marrow endothelial cells. Stem Cells Dev 2012;21:476–486
3. Lee JY, Sohn KH, Rhee SH, Hwang D. Saturated fatty acids, but not unsaturated fatty acids, induce the expression of cyclooxygenase-2 mediated through Toll-like receptor 4. J Biol Chem 2001;276:16683–16689
4. Coenen KR, Gruen ML, Lee-Young RS, Puglisi MJ, Wasserman DH, Hasty AH. Impact of macrophage toll-like receptor 4 deficiency on macrophage infiltration into adipose tissue and the artery wall in mice. Diabetologia 2009;52:318–328
5. Nguyen MT, Favelyukis S, Nguyen AK, et al. A subpopulation of macrophages infiltrates hypertrophic adipose tissue and is activated by free fatty acids via Toll-like receptors 2 and 4 and JNK-dependent pathways. J Biol Chem 2007;282:35279–35292
6. Solinas G, Vilcu C, Neels JG, et al. JNK1 in hematopoietically derived cells contributes to diet-induced inflammation and insulin resistance without affecting obesity. Cell Metab 2007;6:386–397
7. Arkan MC, Hevener AL, Greten FR, et al. IKK-beta links inflammation to obesity-induced insulin resistance. Nat Med 2005;11:191–198
8. Saberi M, Woods NB, de Luca C, et al. Hematopoietic cell-specific deletion of Toll-like receptor 4 ameliorates hepatic and adipose tissue insulin resistance in high-fat-fed mice. Cell Metab 2009;10:419–429
9. Lee YS, Li P, Huh JY, et al. Inflammation is necessary for long-term but not short-term high-fat diet-induced insulin resistance. Diabetes 2011;60:2474–2483
10. Vanhaesebroeck B, Ali K, Bilancio A, Geering B, Foukas LC. Signalling by PI3K isoforms: insights from gene-targeted mice. Trends Biochem Sci 2005;30:194–204
11. Chen D, Mauvais-Jarvis F, Bluher M, et al. p50alpha/p55alpha phosphoinositide 3-kinase knockout mice exhibit enhanced insulin sensitivity. Mol Cell Biol 2004;24:320–329
12. Fruman DA, Cantley LC, Carpenter CL. Structural organization and alternative splicing of the murine phosphoinositide 3-kinase p85 alpha gene. Genomics 1996;37:113–121
13. Ueki K, Yballe CM, Brachmann SM, et al. Increased insulin sensitivity in mice lacking p85beta subunit of phosphoinositide 3-kinase. Proc Natl Acad Sci USA 2002;99:419–424
14. Terauchi Y, Tsuji Y, Satoh S, et al. Increased insulin sensitivity and hypoglycaemia in mice lacking the p85 alpha subunit of phosphoinositide 3-kinase. Nat Genet 1999;21:230–235
15. Terauchi Y, Matsui J, Kamon J, et al. Increased serum leptin protects from adiposity despite the increased glucose uptake in white adipose tissue in mice lacking p85alpha phosphoinositide 3-kinase. Diabetes 2004;53:2261–2270
16. Mauvais-Jarvis F, Ueki K, Fruman DA, et al. Reduced expression of the murine p85alpha subunit of phosphoinositide 3-kinase improves insulin signaling and ameliorates diabetes. J Clin Invest 2002;109:141–149
17. Rabinovsky R, Pochanard P, McNear C, et al. p85 associates with unphosphorylated PTEN and the PTEN-associated complex. Mol Cell Biol 2009;29:5377–5388
18. Park SW, Zhou Y, Lee J, et al. The regulatory subunits of PI3K, p85alpha and p85beta, interact with XBP-1 and increase its nuclear translocation. Nat Med 2010;16:429–437
19. Winnay JN, Boucher J, Mori MA, Ueki K, Kahn CR. A regulatory subunit of phosphoinositide 3-kinase increases the nuclear accumulation of X-box-binding protein-1 to modulate the unfolded protein response. Nat Med 2010;16:438–445
20. Taniguchi CM, Aleman JO, Ueki K, et al. The p85alpha regulatory subunit of phosphoinositide 3-kinase potentiates c-Jun N-terminal kinase-mediated insulin resistance. Mol Cell Biol 2007;27:2830–2840
21. del Rincon J-P, Iida K, Gaylinn BD, et al. Growth hormone regulation of p85alpha expression and phosphoinositide 3-kinase activity in adipose tissue: mechanism for growth hormone-mediated insulin resistance. Diabetes 2007;56:1638–1646
22. Schenk S, McCurdy CE, Philp A, et al. Sirt1 enhances skeletal muscle insulin sensitivity in mice during caloric restriction. J Clin Invest 2011;121:4281–4288
23. Voshol PJ, Jong MC, Dahlmans VEH, et al. In muscle-specific lipoprotein lipase-overexpressing mice, muscle triglyceride content is increased without inhibition of insulin-stimulated whole-body and muscle-specific glucose uptake. Diabetes 2001;50:2585–2590
24. Perreault L, Bergman BC, Hunerdosse DM, Eckel RH. Altered intramuscular lipid metabolism relates to diminished insulin action in men, but not women, in progression to diabetes. Obesity (Silver Spring) 2010;18:2093–2100
25. Crossno JT Jr, Majka SM, Grazia T, Gill RG, Klemm DJ. Rosiglitazone promotes development of a novel adipocyte population from bone marrow-derived circulating progenitor cells. J Clin Invest 2006;116:3220–3228
26. Higgins JA, Jackman MR, Brown IL, et al. Resistant starch and exercise independently attenuate weight regain on a high fat diet in a rat model of obesity. Nutr Metab (Lond) 2011;8:49
27. McCurdy CE, Cartee GD. Akt2 is essential for the full effect of calorie restriction on insulin-stimulated glucose uptake in skeletal muscle. Diabetes 2005;54:1349–1356
28. Fox KE, Fankell DM, Erickson PF, Majka SM, Crossno JT Jr, Klemm DJ. Depletion of cAMP-response element-binding protein/ATF1 inhibits adipogenic conversion of 3T3-L1 cells ectopically expressing CCAAT/enhancer-binding protein (C/EBP) α, C/EBP β, or PPAR γ 2. J Biol Chem 2006;281:40341–40353
29. Kuckleburg CJ, Yates CM, Kalia N, et al. Endothelial cell-borne platelet bridges selectively recruit monocytes in human and mouse models of vascular inflammation. Cardiovasc Res 2011;91:134–141
30. Mira E, León B, Barber DF, et al. Statins induce regulatory T cell recruitment via a CCL1 dependent pathway. J Immunol 2008;181:3524–3534
31. Seitz HM, Camenisch TD, Lemke G, Earp HS, Matsushima GK. Macrophages and dendritic cells use different Axl/Mertk/Tyro3 receptors in clearance of apoptotic cells. J Immunol 2007;178:5635–5642
32. Vanguri P, Farber JM. IFN and virus-inducible expression of an immediate early gene, crg-2/IP-10, and a delayed gene, I-A alpha in astrocytes and microglia. J Immunol 1994;152:1411–1418

33. Li M, Riddle SR, Frid MG, et al. Emergence of fibroblasts with a proinflammatory epigenetically altered phenotype in severe hypoxic pulmonary hypertension. J Immunol 2011;187:2711–2722
34. Spencer M, Unal R, Zhu B, et al. Adipose tissue extracellular matrix and vascular abnormalities in obesity and insulin resistance. J Clin Endocrinol Metab 2011;96:E1990–E1998
35. Cutillas PR, Khwaja A, Graupera M, et al. Ultrasensitive and absolute quantification of the phosphoinositide 3-kinase/Akt signal transduction pathway by mass spectrometry. Proc Natl Acad Sci USA 2006;103:8959–8964
36. Wallerstedt E, Smith U, Andersson CX. Protein kinase C-δ is involved in the inflammatory effect of IL-6 in mouse adipose cells. Diabetologia 2010; 53:946–954
37. Sultan A, Strodthoff D, Robertson AK, et al. T cell-mediated inflammation in adipose tissue does not cause insulin resistance in hyperlipidemic mice. Circ Res 2009;104:961–968
38. Kosteli A, Sugaru E, Haemmerle G, et al. Weight loss and lipolysis promote a dynamic immune response in murine adipose tissue. J Clin Invest 2010; 120:3466–3479
39. Lovren F, Pan Y, Quan A, et al. Adiponectin primes human monocytes into alternative anti-inflammatory M2 macrophages. Am J Physiol Heart Circ Physiol 2010;299:H656–H663
40. Laville M, Auboeuf D, Khalfallah Y, Vega N, Riou JP, Vidal H. Acute regulation by insulin of phosphatidylinositol-3-kinase, Rad, Glut 4, and lipoprotein lipase mRNA levels in human muscle. J Clin Invest 1996;98:43–49
41. Giorgino F, Pedrini MT, Matera L, Smith RJ. Specific increase in p85alpha expression in response to dexamethasone is associated with inhibition of insulin-like growth factor-I stimulated phosphatidylinositol 3-kinase activity in cultured muscle cells. J Biol Chem 1997;272:7455–7463
42. Rieusset J, Chambrier C, Bouzakri K, et al. The expression of the p85α subunit of phosphatidylinositol 3-kinase is induced by activation of the peroxisome proliferator-activated receptor γ in human adipocytes. Diabetologia 2001;44:544–554
43. Rieusset J, Roques M, Bouzakri K, Chevillotte E, Vidal H. Regulation of p85alpha phosphatidylinositol-3-kinase expression by peroxisome proliferator-activated receptors (PPARs) in human muscle cells. FEBS Lett 2001;502: 98–102
44. Abell K, Bilancio A, Clarkson RWE, et al. Stat3-induced apoptosis requires a molecular switch in PI(3)K subunit composition. Nat Cell Biol 2005;7:392–398
45. Cernkovich ER, Deng J, Bond MC, Combs TP, Harp JB. Adipose-specific disruption of signal transducer and activator of transcription 3 increases body weight and adiposity. Endocrinology 2008;149:1581–1590